Multifunctional graphene sensor for detection of environment signals using a decoupling technique

Junyeong Lee, Chang-Ju Lee, Jaewoon Kang, Honghwi Park, Jaeeuk Kim, Muhan Choi, Hongsik Park

PII: S0038-1101(18)30419-2
DOI: https://doi.org/10.1016/j.sse.2018.10.014
Reference: SSE 7482

To appear in: *Solid-State Electronics*

Please cite this article as: Lee, J., Lee, C-J., Kang, J., Park, H., Kim, J., Choi, M., Park, H., Multifunctional graphene sensor for detection of environment signals using a decoupling technique, *Solid-State Electronics* (2018), doi: https://doi.org/10.1016/j.sse.2018.10.014

Multifunctional graphene sensor for detection of environment signals using a decoupling technique

Junyeong Lee[a], Chang-Ju Lee[a], Jaewoon Kang[a], Honghwi Park[a], Jaeeuk Kim[a], Muhan Choi[a], and Hongsik Park[a, *]

[a] School of Electronics Engineering, Kyungpook National University, Daegu, 41566, Korea

Abstract— Graphene is one of good candidates for multifuctional sensors due to its unique material properties, extremely high surface-to-volume ratio and capability of effective co-integration on various substrates. However, the electrical properties of graphene are sensitive to most of typical environment signals such as temperature, light, humidity, and gas. Therefore, for developement of graphene-based multifunctional sensors, it is essential to identify multiple environment information values from the output characteristic of a single graphene sensor. In this study, we developed a temperature-illuminance multifunctional graphene sensor that can identify both tempurature and illumincance values. We also suggest a decoupling technique to precisely identify the temperature and illuminance values from the output characteristic of the sensor that has cross-sensitivity to the both inputs. This decoupling technique is developed based on the different gate-voltage dependence of the temperature- and illumination-induced modulations of the graphene conductivity. The results show that graphene can be used for a material for multifunctional sensors with a proper decoupling technique for indentifying various types of environment signals.

Keywords: graphene; multifunctional sensor; decoupling technique; cross-sensitivity; electrostatic doping;

1. INTRODUCTION

Nowadays, various types of sensors are used for environment monitoring, energy management, health care, feedback control of machines, and so on. To obtain more various environment information, it is generally reguired to increass the number and kinds of individual sensors in sensor systems like a multi sensors module, and it involves the increase of the size, complexity, and cost of sensor modules or systems. An integrated multifunctional sensor can detect the multiple environment signals with relatively less increase of the size, complexity, and cost. Recently, techniques for integration of multiple sensors on a single chip are studied for cost-effective smart sensor applications such as smart home monitoring, road activity monitoring, and weather monitoring [1-4]. For example, Roozeboom *et al.* demonstrated a compact multifunctional sensor chip (2 × 2 mm^2 size) in which 9 individual sensors are integrated for measuring 7 types of environment signals [2]. These multifunctional integrated sensors have been fabricated on Si substrates by using conventional sensing materials and Si based micro-electro-mechanical-system (MEMS) processes.

Graphene is an attractive material to develop various types of sensors due to its outstanding properties such as extremely high surface-to-volume ratio with high mobility, superior flexibility, and capability of effective co-integration on various substrates with relatively simple fabrication process [5-7]. These properties have enabled sensor applications of graphene in artificial electronic skin [8-9], stretchable and flexible sensors [10], human motion sensors [11-13], and so on. Graphene is also widely studied for development of environment sensors because it is sensivite to most of typical environment signals like temperature, illuminance, humidity, pressure, gas, and so on. [5-7, 14-20]. Furthermore, since the single material, graphene, has sensitivity to multiple environment signals simultaenously, graphene has a great potential for being used as a sensing material for multifunctional environment sensors. However, the electrical properties of graphene that are sensitive to multiple environment signals can cause a 'cross-sensitivity' problem that make it hard to identify multiple environment information values from the output characteristic of a single graphene sensor [4]. Therefore, for realization of graphene-based multifunctional sensors, it is essential to develop a decoupling technique for precisely identifying multiple environment signals from a single graphene sensor that has the cross-sensitivity problem.

In this study, we fabricated a multifunctional sensor based on a graphene field-effect transistor (GFET) that could detect temperature and illuminance simultaneously. We also developed a decoupling technique to precisely identify temperature and illuminance values from the output characteristic of the graphene sensor that had severe cross-sensitivity to the both input signals. We evaluated the performance of the multifunctional graphene sensor by comparing the temperature and illumination estimated from the sensor with real environment values.

2. EXPERIMENTAL DETAILS

We fabricated GFETs using polycrystalline graphene that was grown by chemical vapor deposition (CVD) and transferred on SiO_2/Si substrate. The thickness of SiO_2 was 90 nm and the highly p-type doped Si substrate was used as a back-gate of the GFET. After a standard photolithography process with AZ 5214E, source and drain electrodes were patterned by e-beam evaporation of Pd/Au (20/50 nm) film and lift-off process. The graphene channel region was defined by a second photolithography and oxygen plasma etching (30 W, 2 min) process. The photoresist masking layer used for the channel define was removed in 80 °C acetone and rinsed with

* Corresponding author.
E-mail address: hpark@ee.knu.ac.kr (H. Park).

an isopropyl alcohol. The channel width and length of the fabricated device were 50 μm and 40 μm, respectively.

The electrical characteristics of the GFET were measured by a semiconductor parameter analyzer (4155B, Agilent tech., USA) under a high-vacuum condition of 10^{-6} Torr. The GFET was operated with a small drain voltage of 50 mV to minimize a self-heating effect that could change the drain current of the GFET. The sample temperature was precisely controlled in a range from 25 ℃ to 45 ℃ by using by thermal heating system in a vacuum probe station. For characterization of the sensitivity of the GFET to illumination, we used a halogen lamp (3330K, 100W, 6834FO, Philips, Nederland) as a light source which is suitable for testing an illuminance sensor because the radiation spectrum of the lamp is very similar to that of sun light [21-22].

We developed a decoupling technique to identify two different environment information simultaneously from the output of the single graphene sensor. To design the decoupling algorithm, we analyzed temperature- and illuminance-dependence of the current-voltage (I-V) characteristics of the GFET. After the analysis, we selected two specific gate voltages that are suitable for the most effective decoupling of the temperature and illuminance values. Then we measured the drain currents of the device at the selected gate voltages under various conditions of both environment inputs. The drain currents of the GFET were changed by both of environment signals with different sensitivities. We generated the 3-dimensinal (3-D) data maps of both environment signals for drain currents under the two gate voltages by using a scattered interpolation function. Finally, we identified temperature and illuminance values from an arbitrary set of the drain current and gate voltage using the 3-D data maps.

3. Results and Discussions

For a development of the multifunctional graphene sensor, we fabricated a conventional back-gated GFET device. A

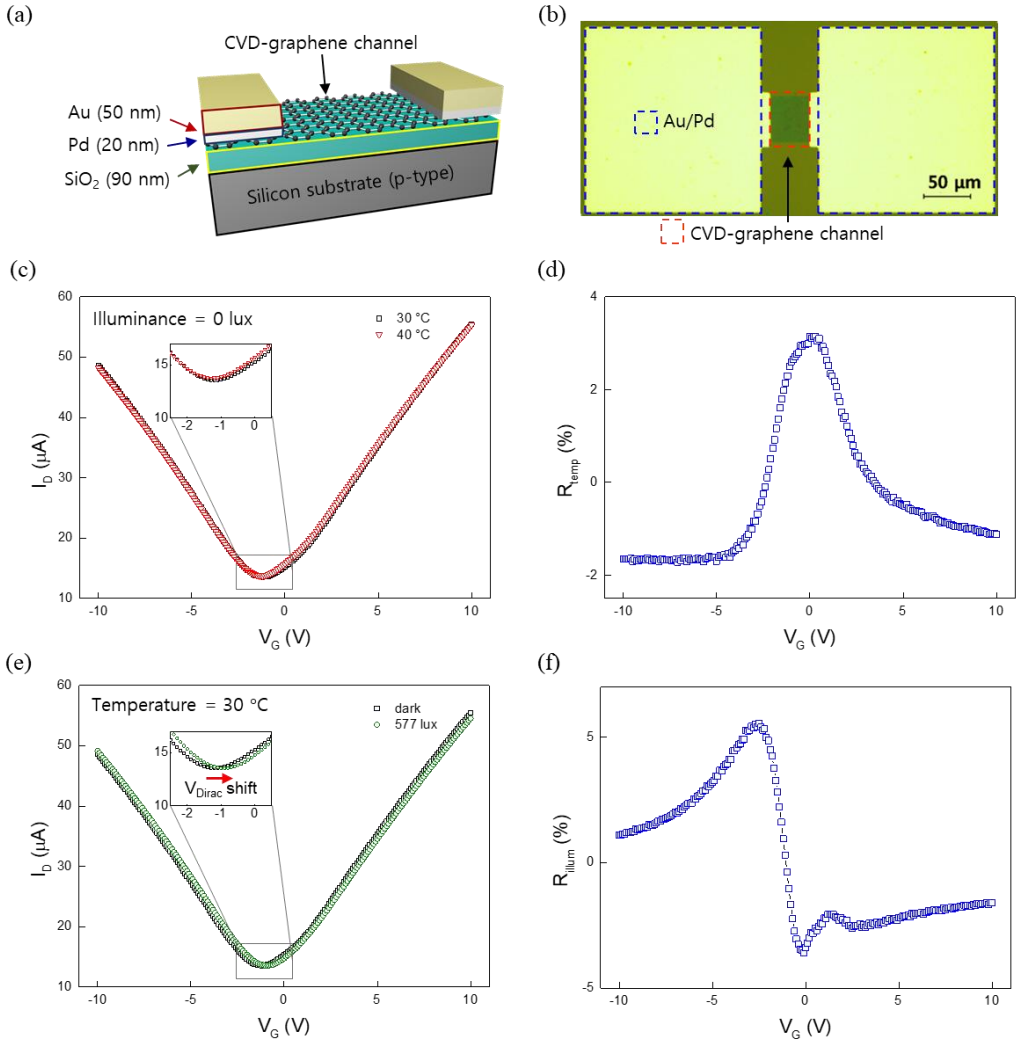

Fig. 1 (a) Schematic and (b) micro-photograph image of the fabricated graphene field-effect transistor (GFET). Scale bar: 50 μm. (c) Transfer characteristics of the GFET measured under two different temperature conditions at dark condition. Inset: transfer characteristics of the GFET near the Dirac voltage (V_{Dirac}) of the device. (d) The conductance-change-ratio of the GFET calculated by the difference between two drain currents measured at 30 ℃ and 40 ℃. (e) Transfer characteristics of the GFET measured under two different illuminance conditions at 30 ℃. Inset: transfer characteristics of the GFET near V_{Dirac} of the device. (f) The conductance-change-ratio of the GFET calculated by the difference between two drain currents measured under illuminance of 0 and 577 lux.

schematic device structure and a micro-photograph image are shown in Fig. 1(a) and (b), respectively. Firstly, we measured the electrical characteristics of the fabricated GFET under different temperature conditions. The plots of drain currents (I_D) as a function of the gate voltage (V_G) under the different temperature conditions are shown in Fig. 1(c). I_D is increased at higher temperature when the gate bias is close to Dirac voltage (V_{Dirac}). The reason of the negative temperature coefficient of resistance (TCR) near V_{Dirac} is that the carrier concentration of graphene is very low and thermally generated carriers can dominantly affect the conductivity of graphene [23]. On the other hand, when graphene is highly doped by a large gate bias, the temperature dependence of the device conductance is reversed because the metallic behavior is dominant and TCR is positive in this condition [23]. The temperature sensitivity of this device was dependent on the gate bias. Fig. 1(d) shows the conductance-change-ratio by temperature (R_{temp}) under varying gate bias, which is defined by

$$R_{temp} = \frac{I_{D,40\,℃} - I_{D,30\,℃}}{I_{D,30\,℃}} \times 100 \quad (1)$$

where $I_{D,40\,℃}$ and $I_{D,30\,℃}$ are the drain currents measured under temperature of 40 °C and 30 °C, respectively. The illuminance was maintained at 0 lux and the drain voltage was fixed at 50 mV. The maximum R_{temp} was observed near 0 V gate bias. We also measured the electrical characteristics of the GFET under different illumination conditions to investigate difference in the temperature- and illumination-dependence of the $I_D - V_G$ characteristics. The plots of I_D as a function of V_G under the different illuminance conditions are shown in Fig. 1(e). Fig. 1(f) shows the conductance-change-ratio by illuminance (R_{illum}) under varying gate bias, which is defined by

$$R_{illum} = \frac{I_{D,577\ lux} - I_{D,0\ lux}}{I_{D,0\ lux}} \times 100 \quad (2)$$

where $I_{D,577\ lux}$ and $I_{D,0\ lux}$ are the drain currents measured under illuminance of 577 lux and 0 lux, respectively. The temperature was maintained at 30 °C and the drain voltage was fixed at 50 mV. Unlike the case of the temperature-dependent $I_D - V_G$ characteristic, the shape of $I_D - V_G$ curve under illumination was not significantly changed except for the shift of V_{Dirac} as shown in the inset of Fig. 1(e), as reported several literatures related to graphene photodetectors [24-26]. Due to this characteristic of illuminance-induced conductance modulation, a gate voltage corresponding to $R_{illum} = 0$ exist at the cross point of the $I_D - V_G$ curves under dark and illuminance conditions. The maximum R_{illum} is observed near V_{Dirac}. As shown Fig. 1(c) – (f), the drain current of the GFET is changed by both of temperature and illuminance change. These $I_D - V_G$ characteristics indicate that the temperature or illuminance cannot be defined independently by monitoring a single output (drain current) of the device. Therefore, it is essential to use a decoupling technique for identify two environment signals from the single device. We designed a decoupling technique based on the fact that the device showed the difference in the temperature- and illuminance-dependent $I_D - V_G$ characteristic. The decoupling technique consists of four steps: (i) selecting two specific gate voltages (V_{G1} and V_{G2}) that are suitable for effectively decoupling temperature and illuminance values from corresponding drain currents (I_{D1} and I_{D2}), (ii) obtaining training data sets (I_{D1}, I_{D2}) that is measured with known temperature and illuminance conditions and grouping training data obtained at the same temperature or illuminance condition in the $I_{D1} - I_{D2}$ plot, (iii) generating all fitting functions for all grouped training-data-sets and defining decoupling reference points that are the intersection points of temperature-fitting functions and illuminance-fitting functions, and (iv) creating a decoupling algorithm that can define the temperature and illuminance values from an arbitrary measured-data set (V_{G1}, I_{D1}, V_{G2}, I_{D2}) by using the decoupling reference points.

Since the temperature and illuminance values cannot be separately identified from a single drain current value, it is required to get two different drain current values at different gate voltages for decoupling two environment information. Therefore, it is important to select appropriate two gate voltages for effective decoupling. To select the gate voltage values, we considered three criteria. First, it is desirable to select two gate biases: the first gate voltage (V_{G1}) corresponding to a maximized temperature-illuminance relative sensitivity and the second gate voltage (V_{G2}) corresponding to a minimized relative sensitivity, where the temperature-illuminance relative sensitivity is defined by R_{temp} and R_{illum}

$$R_{T/I} = \frac{R_{temp}}{R_{illum}} \quad (3)$$

This means that a GFET sensor has a high (low) sensitivity to temperature (illuminance) at V_{G1} and a high (low) sensitivity to illuminance (temperature) at V_{G2}. Second, the gate voltage should be selected in a proper range for the graphene channel of the GFET to absorb all range of the visible light spectrum. If the Fermi energy (energy gap between Fermi level (E_F) and Dirac point (E_{Dirac})) of graphene is larger than half of incident photon energy ($h\nu/2$), photon-absorption efficiency of graphene becomes very low [27]. We used a halogen lamp for photoresponse measurement and this light source has a visible spectrum that is usually defined in the range of 400 ~ 700 nm wavelength [28]. Since the wavelength of visible light is smaller than 700 nm, the Fermi energy should be smaller than 0.89 eV. The Fermi energy is determined by gate voltage, gate capacitance, and Dirac voltage as given by following equation.

$$\text{Fermi energy} = \hbar v_F \sqrt{\pi n} = \hbar v_F \sqrt{\pi C_{ox} \frac{(V_G - V_{Dirac})}{e}} \quad (4)$$

In this experiment, we used a 90-nm-thick SiO_2 for the gate insulator and V_{Dirac} was -1.2 V; therefore, the gate voltage for illuminance sensing had to be selected in a range of -5.5 ~ 3.1 V. Third, we could not select a gate bias that is too close to V_{Dirac} because the R_{illum} was too abruptly changed by illuminance intensity near V_{Dirac}, which was not desirable for a stable sensor operation and signal decoupling.

Based on the criteria mentioned above, we selected V_{G1} of 0 V for temperature sensing and V_{G2} of -2 V for illuminance sensing. The next step is to obtain training data sets for generating the decoupling algorithm. We measured I_{D1} at V_{G1} and I_{D2} at V_{G2} under various temperature and illuminance conditions (training data sets). In the measurement, the temperature conditions were 25, 35, 45 °C and the illuminance conditions were 0, 45, 93, 227, 450, 577 lux. The drain voltage was fixed at a low voltage of 50 mV to prevent an additional

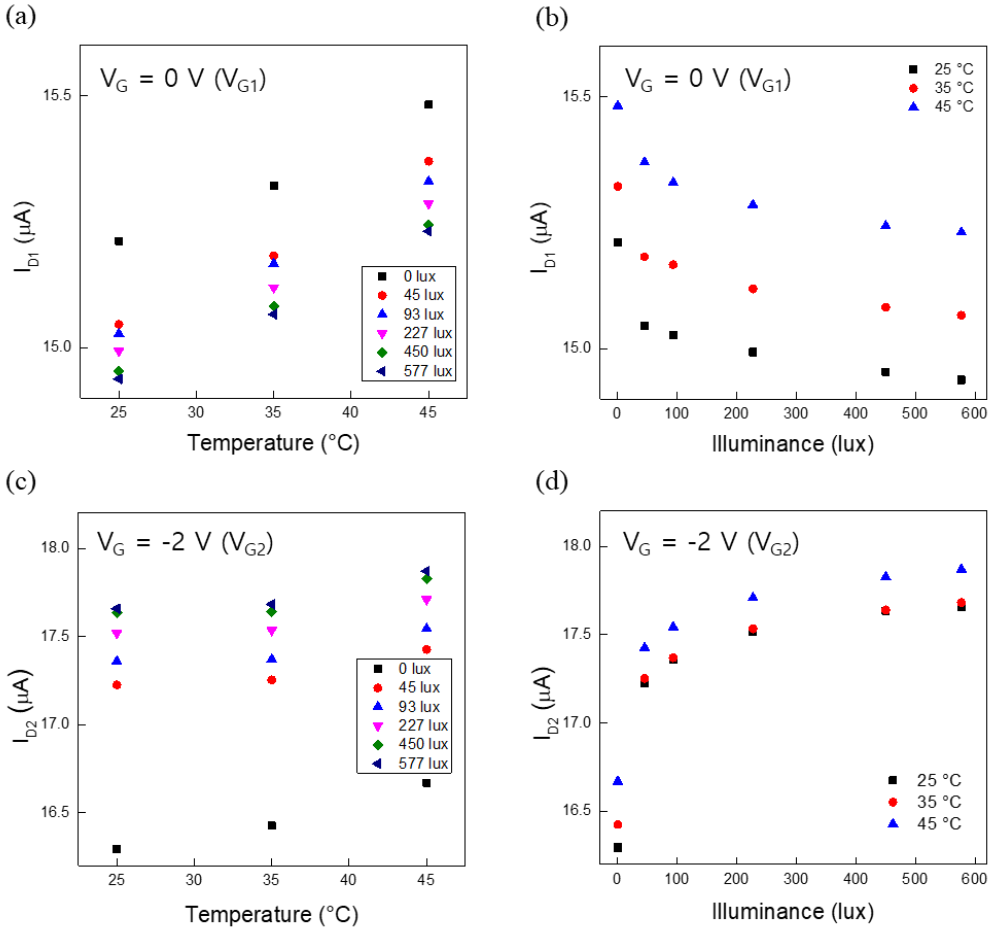

Fig. 2 Output drain currents of the GFET at two selected gate voltages. (a) Drain current values versus temperature under various illuminance conditions at V_G = 0 V (V_{G1}) and (b) drain current values versus illuminance under different temperature conditions at V_G = 0 V (V_{G1}). (c) Drain current values versus temperature under various illuminance conditions at V_G = -2 V (V_{G2}) and (d) drain current values versus illuminance under different temperature conditions at V_G = -2 V (V_{G2}).

heating effect by a large drain current. Fig. 2(a) and (b) show the drain currents (I_{D1}) measured at V_G = 0 V (V_{G1}) plotted as a function of different temperature and illuminance conditions, respectively. Similarly, plots of the drain currents (I_{D2}) measured at V_{G2} are shown in Fig. 2(c) and (d) as a function of different temperature and illuminance conditions, respectively. As indicated by Fig. 1(d) and (f), Fig. 2 also clearly shows that temperature and illuminance cannot be defined simultaneously from a single drain current value. However, as expected, temperature and illuminance could be defined by a set of drain current (I_{D1}, I_{D2}) since the drain current had different values and temperature-/illuminance-sensitivities at V_G = 0 V and -2 V. As shown in Fig. 2(a) and (b), the drain current at V_{G1} was more sensitive to temperature change than illuminance change. On the other hand, the drain current at V_{G2} was more sensitively changed by illuminance than temperature as shown in Fig. 2(c) and (d).

The drain currents measured at V_G = 0 V and -2 V were plotted in the $I_{D1} - I_{D2}$ graph as shown in Fig. 3(a). Each (I_{D1}, I_{D2}) point is a training data corresponding to a specific set of temperature and illuminance value. The training data are clearly separated and well-distributed in the 2-dimensional (2-D) domain, which indicates that V_{G1} and V_{G2} are adequately selected. The well-distributed training data could be grouped as a training data set by all temperature or illuminance condition. For example, the training data sets grouped by temperature are marked by the dotted lines in Fig. 3(a). We generated fitting functions corresponding to all training data sets grouped by the environment values. A fitting function corresponding to a training data set of a specific temperature (or illuminance) gives the illuminance-dependence (or temperature-dependence) of (I_{D1}, I_{D2}) set at the given temperature (or illuminance). The fitting curves generated from the training data (blue squares) are shown in Fig. 3(b). Green lines (Red lines) are the fitting functions corresponding to the training data set under the same temperature (illuminance). The illuminance-dependence (green lines) of (I_{D1}, I_{D2}) points was well fitted by an exponential model and the temperature-dependence (red lines) was well fitted by a second-order polynomial model with high fitting accuracies (R^2 > 0.997), where R^2 is the coefficient of determination evaluating the accuracies of a fitting function [29].

Using the fitting functions and a proper interpolation method, we can define (I_{D1}, I_{D2}) values corresponding to arbitrary environment information. For defining temperature and illuminance values of (I_{D1}, I_{D2}) points between all fitting functions, we used decoupling reference points that are the intersection points of the temperature-fitting functions and illuminance-fitting functions. The decoupling reference points are marked by the symbol 'X' in Fig. 3(b). To use the linear

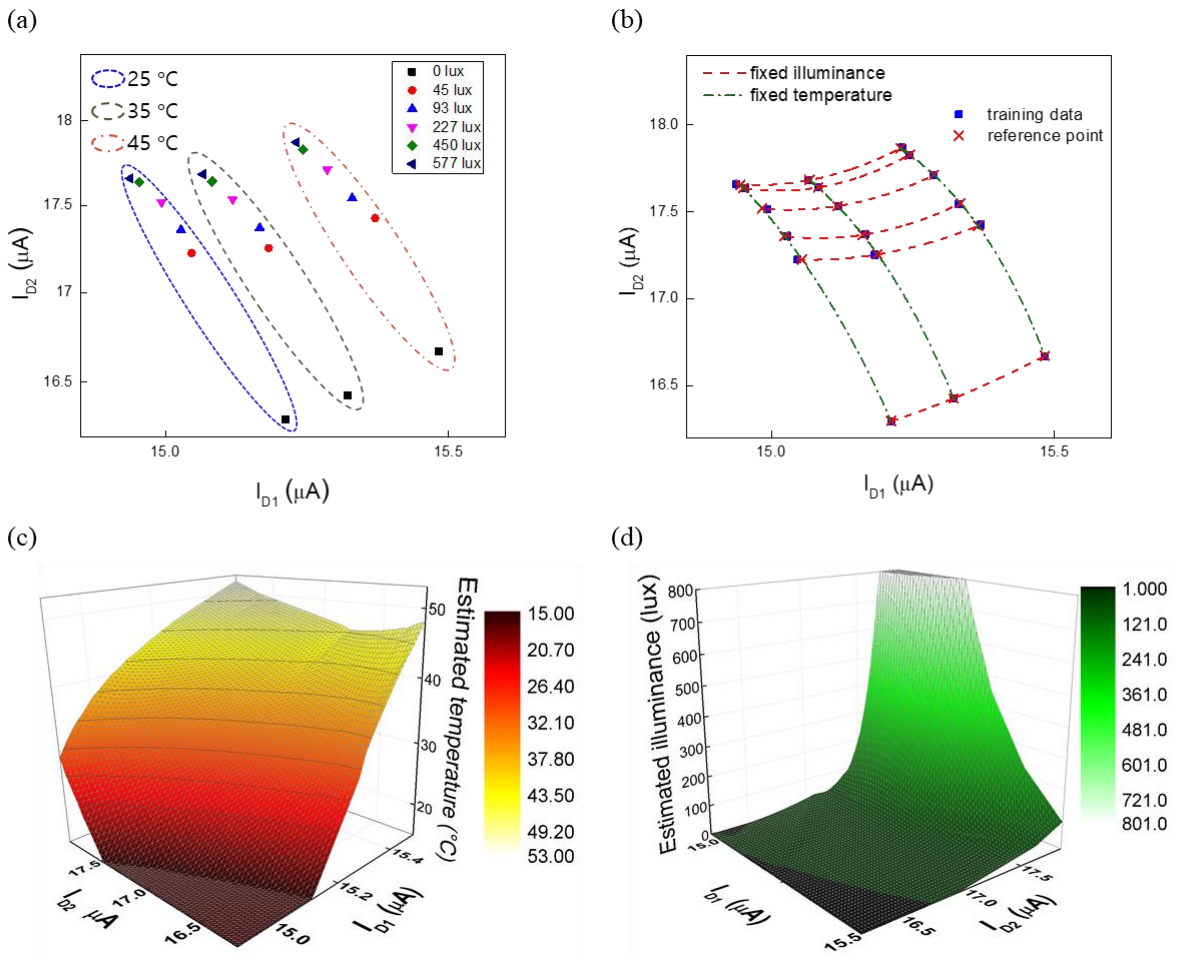

Fig. 3 (a) The plotting result of the training data ($I_{D1} - I_{D2}$) in 2-D domain. (b) The fitting function generation results and defining of decoupling reference points for creating a decoupling algorithm. 3-D data mapping results for estimation of (c) temperature value and (d) illuminance value from an arbitrary measured-data set (V_{G1}, I_{D1}, V_{G2}, I_{D2}) by using the decoupling algorithm with the decoupling reference points.

interpolation method with a high estimation accuracy, we generated additional 9 fitting functions between the adjacent initial curved fitting functions and defined 117 additional decoupling reference points between adjacent four initial decoupling reference points. Then, based on the linear interpolation from the dense decoupling reference points, we could generate (I_{D1}, I_{D2}) values corresponding to all arbitrary sets of temperature and illuminance conditions. Therefore, by using the developed decoupling algorithm, the temperature and illuminance values can be defined from the sets of two drain currents as shown by the 3-D temperature and illuminance maps in Fig. 3(c) and (d).

We verified the performance of the fabricated GFET sensor and the capability of the developed decoupling technique by evaluating the accuracy of the environment values estimated from sensor output signals. For this evaluation, we measured drain current data at V_{G1} and V_{G2} under known environment conditions which are different from temperature and illuminance set used for training data, and we compared the environment signal values estimated from the measured currents with the known values. In this study, a drain current value used for performance evaluation is called a test data. For evaluation, we measured the drain currents at V_{G1} = 0 V and V_{G2} = -2 V under temperature conditions of 30, 40 °C with varying illuminance (0, 45, 93, 227, 450, 577 lux). We extracted temperature and illuminance values from the measured test data based on the decoupling algorithm identifying an environment information set for an arbitrary drain current set (as shown by the 3-D maps in Fig. 3(c) and (d)). Fig. 4(a) shows the temperature and illuminance values that are defined from decoupling reference points (obtained from the training data) and estimated from the test data. The error rates in the illuminance (and temperature) estimation of the sensor is shown in histogram of Fig. 4(b) (and Fig. 4(c)). The error rate was calculated from the difference between the estimated environment values and the known values. The average error rate in the estimation of illuminance by this sensor and decoupling technique was 3.5 %. As shown in Fig. 4(a), the illuminance error rate was relatively large at high intensity of illuminance. We think that this is attributed to the low device sensitivity to illuminance at a high intensity region (larger Δilluminance/ΔI_D), which could cause a large estimation error by measurement and decoupling calculation errors. The average error rate in the estimation of temperature by this sensor and decoupling technique was 3.9 %. The overall values of the estimated temperature were slightly larger than the known temperature values. We think that the decoupling accuracy can be further improved by increasing the number of

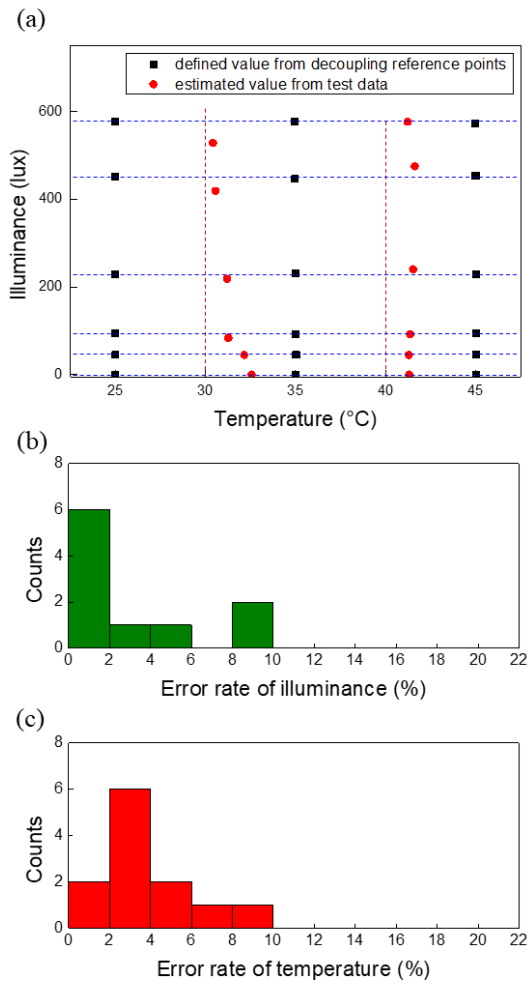

Fig. 4 Evaluation of the accuracy of the environment values estimated from the sensor outputs. (a) Temperature and illuminance values defined from the decoupling reference points (black squares) and estimated from the test data (red circles). Error rates of the estimated (b) illuminance and (c) temperature values calculated from the difference between the estimated environment values and the known values.

training data sets. These results show that the developed decoupling technique can be used to identify two environment information values simultaneously from the output current sets of a single GFET.

4. Conclusion

We developed a multifunctional graphene sensor based on a GFET structure for detection of two environment information, temperature and illuminance, simultaneously. We also designed a decoupling technique by using a different gate-voltage dependence of the device sensitivity to temperature and illuminance. By selection of two proper gate biases, we could obtain the output drain currents that are modulated by temperature and illuminance with different relative sensitivities. By using the decoupling algorithm based on the curve fitting and interpolation methods, we could identify two environment information values from the drain currents of the single GFET sensor with an average error rate lower than 4 %. This result shows that graphene could be used as a sensing material for multifunctional sensor with a proper decoupling technique.

References

[1] Ni Z, Yang C, Xu D, Zhou H, Zhou W, Li T, et al. Monolithic Composite "Pressure + Acceleration + Temperature + Infrared" Sensor Using a Versatile Single-Sided "SiN/Poly-Si/Al" Process-Module. Sensors 2013;13:1085-101.
[2] Roozeboom CL, Hill BE, Hong VA, Ahn CH, Ng EJ, Yang Y, et al. Multifunctional Integrated Sensors for Multiparameter Monitoring Applications. J of Microelectromech Syst 2015;24:810-21.
[3] Zhang Y, Yang C, Meng F, Liu G, Gao C, Hao Y. A Monolithic Integration Multifunctional MEMS Sensor Based on Cavity SOI Wafer. in Proc IEEE Sensors 2014;1952-55.
[4] Huang L, Zhang Z, Chen ZLB, Ma X, Dong L, Peng LM. Multifunctional Graphene Sensors for Magnetic and Hydrogen Detection. ACS Appl Mater Interfaces 2015;7:9581-88.
[5] Rao CN, Sood AK, Subrahmanyam KS, Govindaraj A. Graphene: The New Two-Dimensional Nanomaterial. Angew Chem 2009;48:7752-77.
[6] Novoselov KS, FalKo VI, Colombo L, Gellert PR, Schwab MG, Kim K. A Roadmap for Graphene. Nature 2012; 490:192-200.
[7] He Q, Wu S, Yin Z, Zhang H. Graphene-based Electronic Sensors. Chem Sci 2012;3:1764-72.
[8] Wang Y, Wang L, Yang T, Li X, Zang X, Zhu M, et al. Wearable and Highly Sensitive Graphene Strain Sensors for Human Motion Monitoring. Adv Funct Mater 2014;24:4666-70.
[9] Yang T, Wang W, Zhang H, Li X, Shi J, He Y, et al. Tactile Sensing System Based on Arrays of Graphene Woven Microfabrics: Electromechanical Behavior and Electronic Skin Application. ACS NANO 2015;9:10867-75.
[10] Li X, Zhang R, Yu W, Wang K, Wei J, Wu D, et al. Stretchable and highly sensitive graphene-on-polymer strain sensors. Sci Rep 2012;2:870.
[11] Lee M, Chen CY, Wang SH, Cha SN, Park YJ, Kim JM, et al. A Hybrid Piezoelectric Structure for Wearable Nanogenerators. Adv Mater 2012;24:1759-64.
[12] Lee J, Lee KY, Gupta MK, Kim TY, Lee D, Ryu C, et al. Highly Stretchable Piezoelectric- Pyroelectric Hybrid Nanogenerator. Adv Mater 2013;26:765-9.
[13] Cai L, Song L, Luan P, Zhang Q, Zhang N, Gao Q, et al. Super-stretchable, Transparent Carbon Nanotube-Based Capacitive Strain Sensors for Human Motion Detection. Sci Rep 2013;3:3048.
[14] Shi R, Xu H, Chen B, Zhang Z, Peng LM. Scalable Fabrication of Graphene Devices through Photolithography. Appl Phys Lett 2013;102: 113102.
[15] Kenichi L, Ishikawa. Nonlinear optical response of graphene in time domain. Phys Rev B 2010:82:201402.
[16] Furchi M, Urich A, Pospischil A, Lilley G, Unterrainer K, Detz H, et al. Microcavity-Integrated Graphene Photodetector. Nano Lett 2012;12: 2773-7.
[17] Xu W, Petters FM, Lu TC. Dependence of resistivity on electron density and temperature in graphene. Phys Rev B 2009;79:073403.
[18] Feng T, Xie D, Li G, Xu J, Zhao H, Ren T, et al. Temperature and gate voltage dependent electrical properties of graphene field-effect transistors. Carbon 2014;78:250-6.
[19] Gautam M, Jayatissa AH. Gas Sensing Properties of Graphene Synthesized by Chemical Vapor Deposition. Mater Sci Eng C 2011;31: 1405-11.
[20] Park SJ, Kwon OS, Lee SH, Song HS, Park TH, Jang J. Ultrasensitive Flexible Graphene Based Field-Effect Transistor (FET)-Type Bioelectronic Nose. Nano Lett 2012;12:5082-90.
[21] Tsuei CH, Pen JW, Sun WS. Simulating the illuminance and the efficiency of the LED and fluorescent lights used in indoor lighting design. Opt Express 2008;16:18692-701.
[22] Lavery LL, Whiting GL, Arias AC. All ink-jet printed polyfluorene photosensor for high illuminance detection. Organic Electron 2011;12:682-685.
[23] Heo J, Chung HJ, Lee SH, Yang H, Seo DH, Shin JK, et al. Nonmonotonic temperature dependent transport in graphene grown by chemical vapor deposition. Phys Rev B 2011;84:035421.
[24] Ishida S, Anno Y, Takeuchi M, Matsuoka M, Takei K, Arie T, et al. Highly photosensitive graphene field-effect transistor with optical memory function. Sci Rep 2015;5:15491.
[25] Yoo TJ, Kim JY, Lee SK, Kang CG, Chang KE, Hwang HJ, et al. Zero-Bias Operation of CVD Graphene Photodetector with Asymmetric Metal Contacts. ACS Photonics 2018;5:365-70.
[26] Xia F, Mueller T, Lin Y, Valdes-Garcia A, Avouris P. Ultrafast graphene photodetector. Nat Nanotech 2009;4:839-43.

[27] Liu M, Yin X, Ulin-Avila E, Geng B, Zentgraf T, Ju L, et al. A graphene-based broadband optical modulator. Nature 2011;474:64-7.
[28] Pal GK, Pal P. Textbook of Parctical Physiology. 2nd ed. Chennai: Orient Longman; 2002.
[29] Renaud O, Victoria-Feser M. A robust coefficient of determination for regression. J Stat Plan Inference 2010;7:1852-62.

1. Junyeong Lee		5. Jaeeuk Kim	
2. Chang-Ju Lee		6. Muhan Choi	
3. Jaewoon Kang		7. Hongsik Park	
4. Honghwi Park			

1. Junyeong Lee received the bachelor's degree from Kyungpook National University, Daegu, South Korea, in 2012, and the master's degree from Kyungpook National University, Daegu, South Korea, in 2015. He is currently pursuing the Ph.D degree at Kyungpook National University. His research interests are focused on sensor applications and algorithms.	5. Jaeeuk Kim received the bachelor's degree from Kyungpook National University, Daegu, South Korea, in 2016, and the master's degree from Kyungpook National University, Daegu, South Korea, in 2018. He is currently employee at SK Hynix.
2. Chang-Ju Lee received the bachelor's degree from Kyungpook National University, Daegu, South Korea, in 2010, and the master's degree from Kyungpook National University, Daegu, South Korea, in 2012. He is currently pursuing the Ph.D degree at Kyungpook National University. His research interests are focused on monolithic Si-photonic chips and optoelectronic devices	6. Muhan Choi is currently an associate professor at the School of Electronics Engineering in Kyungpook National University (KNU). He received the Ph.D. degree from Sogang Univ. in 2003. From 2005 to 2008, he was a postdoctoral researcher in Advance Telecommunication Research Institute International (ATR) in Kyoto, Japan. From 2009 to 2010, he was a senior researcher in Korea Advanced Institute of Science and Technology (KAIST). Prior to joining KNU, he worked as a senior researcher in Electronics Telecommunication Research Institute (ETRI) for 2 years. His main research interest is in the development of micro/nano photonics device based on metamaterial and active device for terahertz imaging
3. Jaewoon Kang received the bachelor's degree from Kyungpook National University, Daegu, South Korea, in 2015, and the master's degree from Kyungpook National University, Daegu, South Korea, in 2017. He is currently pursuing the Ph.D degree at Kyungpook National University. His research interests are focused on nanomaterial-based device and microfluidic chips.	7. Hongsik Park* received the Ph.D. degree from Brown University in 2011. He was a researcher at Samsung Advanced Institute of Technology, Korea from 1999 to 2006. He also worked at IBM T. J. Watson Research Center as a research staff member from 2011 to 2014. He is currently an associate professor at the School of Electronics Engineering at Kyungpook National University, Korea. His research interests are focused on integration of nanomaterial-based devices with conventional Si devices for Si photonics and integrated sensor applications.
4. Honghwi Park received the bachelor's degree from Kyungpook National University, Daegu, South Korea, in 2016. He is currently pursuing the Combined MS/Ph.D degree at Kyungpook National University. His research interests are focused on photodetectors and optical modulators.	

Highlights

► A multifunctional sensor based on GFET is fabricated for detecting temperature and illuminance information, simultaneously.
► A decoupling technique is developed to identify two environment signals from the output of the fabricated GFET, regardless of cross-sensitivity.
► Results of experiment show that the developed decoupling technique can be used to identify two environment information values from the output of the single GFET and that graphene could be used as a sensing material for a multifunctional sensor when combined with an appropriate decoupling technique.